Journal of Power Sources 442 (2019) 227253

Contents lists available at ScienceDirect

Journal of Power Sources

journal homepage: www.elsevier.com/locate/jpowsour

Optimization of pulse current on energy storage of zinc-air flow batteries

Tien-Fu Yang [a,b], Jian-Hong Lu [a,b], Wei-Mon Yan [a,b,**], Mohammad Ghalambaz [c,d,*]

[a] Department of Energy and Refrigerating Air-Conditioning Engineering, National Taipei University of Technology, Taipei, 10608, Taiwan
[b] Research Center of Energy Conservation for New Generation of Residential, Commercial, and Industrial Sectors, National Taipei University of Technology, Taipei, 10608, Taiwan
[c] Department for Management of Science and Technology Development, Ton Duc Thang University, Ho Chi Minh City, Vietnam
[d] Faculty of Applied Sciences, Ton Duc Thang University, Ho Chi Minh City, Vietnam

ARTICLE INFO

Keywords:
Zinc-air flow battery
Pulse current
Energy storage
Taguchi method

ABSTRACT

The energy storage of a zinc-air flow battery subject to a pulse current is experimentally addressed. The energy storage occurs in the form of zinc reduction during the charging process. The controlling parameters, affecting the zinc reduction, are an electrolyte temperature, a pulse current, a pulse frequency, and a duty cycle. A pulse current provides more controlling parameters compared to a uniform DC current. The Taguchi method is used to optimize the control parameters and maximize zinc reduction and energy storage efficiency. Five levels for four control parameters are adopted in the Taguchi method, and an L25 orthogonal table is introduced for experimental tests. The optimum set of control parameters is obtained as temperature 40 °C, current 1.4 A, pulse frequency 50 Hz, and duty cycle 85%. In this case, 3.668g zinc is produced during 1 h of charging process. By using the pulse current, the weight of produced zinc particles is increased up to 1.394g by compared to the regular DC current. Therefore, using pulse current parameters does contribute to the improvement of energy storage efficiency. Finally, the SEM study of the produced zinc particles demonstrates that employing a pulse current provides finer zinc particles compared to a DC current.

1. Introduction

Since the late 1990s, lithium-ion batteries (LIBs) have been widely developed and utilized as the rechargeable batteries in the global market. However, there are significant disadvantages in the practical application of LIBs, such as high costs, environmental issues, fire hazard concerns, and battery recycling problems [1]. Moreover, there is a continuous demand for the development of new electrochemical systems with higher energy density than current batteries, particularly for emerging markets in electromobility and large-scale stationery [2]. This is while the conventional LIBs technology, based on intercalation chemistry, is approaching its performance limit [3]. In the growing demand for high-performance and safe energy storage technologies, development of metal-air batteries is one of the new promising technologies [4]. The metal-air batteries provide a higher energy density compared to Li-ion batteries. Moreover, metal-air batteries benefit from abundant materials with improved safety [5]. The practical application of metal-air batteries is under development, and significant progress has been made so far. However, future optimization and advancement of these batteries are demanded before they could be widely commercially viable [4].

Metal-air batteries are consisting of a bi-functional air electrode, an electrolyte solution, and a metal electrode. The electrolyte can be aqueous or non-aqueous, and the metal electrode can be made of Zn, Al, Mg, or Li. Metal-air batteries oxidize the metal electrode by using the available oxygen in the air, and they reversibly form solid metal-oxides [2,4]. The weight of metal-air batteries can be notably lower than that of LIBs [4]. Conventional batteries heavy active materials as reactant which made them heavy, but the metal-air batteries utilize the atmospheric oxygen in the cathode as the electrochemical reactant, which reduces the weight of metal-air batteries significantly [6,7]. Among rechargeable metal-air batteries, zinc–air systems, are considered one of the most promising candidates since zinc is inexpensive and abundant. The electrodeposition of zinc is relatively easy in aqueous electrolytes [2]. Moreover, zinc is the most common anode material in primary metal-air batteries due to its low cost and high capacity [8]. A zinc-air battery is typically composed of four main components: a zinc electrode, an alkaline electrolyte, an air electrode, and a separator [8]. The

* Corresponding author. Ton Duc Thang University, Ho Chi Minh City, Vietnam.
** Corresponding author. Department of Energy and Refrigerating Air-Conditioning Engineering, National Taipei University of Technology, Taipei, 10608, Taiwan.
E-mail addresses: wmyan@ntut.edu.tw (W.-M. Yan), mohammad.ghalambaz@tdtu.edu.vn (M. Ghalambaz).

https://doi.org/10.1016/j.jpowsour.2019.227253
Received 18 July 2019; Accepted 1 October 2019
Available online 7 October 2019
0378-7753/

air electrode is typically made of a catalyst-painted gas diffusion layer. The method of storage and the reaction process is relatively simple. The oxidation reaction of zinc generates electrical energy, and the reduction reaction of zinc oxide stores the electrical power. The zinc-air batteries can be divided into three categories. Conventional planar batteries [9,10] with quiescent electrolyte, flow batteries [11,12] with a circulation of electrolyte, and flexible batteries [13,14] which mainly benefit from a solid-state electrolyte, which is flexible mechanically.

The literature review concerning zinc-air batteries shows that most of the charging and discharging systems are integrated into one body, which causes various problems such as low efficiency and unwanted gas generation. Moreover, air can be easily pierced by the dendritic zinc structure. The discharge module and the charging module can be designed and operated separately to avoid the mentioned problems. In a separated charging-discharging design, the transported zinc particles and zinc oxide are repeatedly recycled between the charging and discharging modules through the flowing electrolyte, as shown in Fig. 1. The advantage of this design is that the zinc oxide reduction process is not carried out inside the battery. The gas and dendritic zinc structure generated during the zinc oxide reduction process will not cause damage to the battery frame, and the produced gas can be eliminated without concerns. Moreover, the separation of the charging module simplifies the design mechanism of the battery, required material, and increases the cycle life of zinc anode.

Regarding zinc-air batteries with separate charging and discharging modules, the reduction of zinc from zinc oxide is quite important. The literature review shows that there are various parameters, which influence the zinc reduction during the electrodeposition process. The electrolyte temperature, the operating voltage, the current density, and the electrodeposition time are major parameters which can control the zinc deposition, surface morphology, and the structure of the produced zinc particles.

The effect of electrolyte temperature on the electroplated metals is investigated in some of past researches. For instance, Sahaym et al. [15] electroplated tin on a copper plate at a current density of 50 mA/cm^2 in an alkaline electrolyte. The electrolyte temperature was between 35 °C and 85 °C while the plating time was 240 s. The surface morphology of the electroplated samples at different temperatures was investigated using a Scanning Electron Microscope (SEM). The results showed that an increase in the electrolyte temperature enhances the smoothness of the underlying surface. Jinlong et al. [16] employed a direct current (DC) current for reduction of nickel at three temperature of 20 °C, 50 °C, and 80 °C. The outcomes show that the increase of the electrolyte temperature slightly reduces the nickel grain size. Yamaguchi et al. [17] deposited bismuth telluride (Bi_2Te_3) thin films in an electrolyte within the temperature range of 10 °C–70 °C. It is found that a rise in the temperature enhances the deposition rate. The increase of the temperature from 10 °C to 80 °C intensifies the deposition rate by three fold. The literature review shows that the operating temperature of the electrolyte influences the diffusion rate of metal ions in the electrolyte, which in turn, it changes the surface morphology of the coating and the reduced metal grain size. The effect of current density on the electrodeposition behavior of metal oxides has been addressed in some of the recent investigations. Kazazi [18] deposited manganese dioxide (MnO_2) on a graphite substrate at room temperature and various anodic current densities. The electrolyte was containing 0.1 M manganese acetate ($Mn(CH3COO)_2$) and 0.05 M sodium acetate ($C_2H_3NaO_2$). The applied current density was 1.5 and 25 mA/cm^2. The results show that the film deposited by 25 mA/cm^2 forms a porous structure with small nanoparticles, which increases the specific surface area of the substrate. Consequently, the produced film structure enhances electrochemical performance.

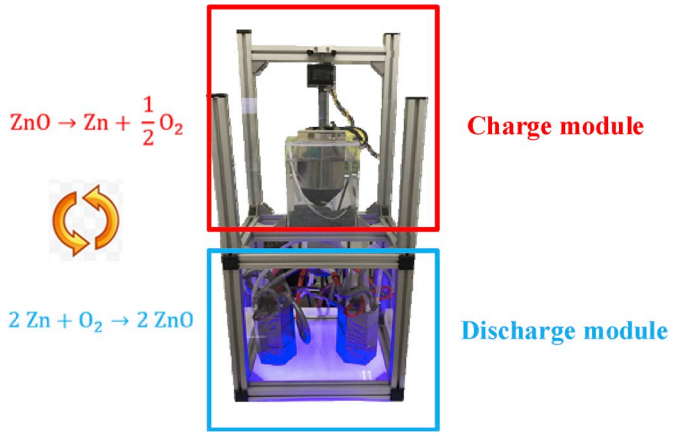

Fig. 1. A view of separated charging and discharging modules in a zinc-air flow battery.

Kumar and Prasad [19] deposited iron in an electrolytic bath of ferrous chloride. The deposited surface was investigated at two different average current densities of 32 mAcm^{-2} and 64 mAcm^{-2}. It was found that an increase in the applied voltage can promote the nucleation rate. Upon doubling the current density, the grain size reduced from 16 μm to 6 μm. The literature review shows that the increase of the electrodeposition current density enhances the electrochemical performance and also affects the surface morphology. However, when the current density threshold is exceeded, the electrodeposition quality may be notably reduced due to the hydrogen evolution phenomenon. A novel approach for zinc recovery in zinc-air batteries is employing a pulse plating. Pulse plating is a method of electroplating by inputting a voltage or current that changes periodically with the time. In a pulse plating process, the voltage and current values are rapidly alternated between two different values to form a current having the same amplitude, application time, and polarity. The pulse plating has been utilized in various applications, including electrodeposition of tin-copper alloys [20], NiP alloy coatings [21], nickel-ceramic lithium electrodeposition [22], and CuInGaSe2 thin films [23]. The pulse can be in various waveforms, including square waves, sine waves, saw-tooth waves, and triangular waves, where square waves are the most common pulse waveforms. In a traditional DC plating, only the voltage and the current can be changed to control the plating process. The advantage of pulse plating is that there are more variables, which can be changed. The variable of a pulse plating can be pulse current density, peak current density, pulse duration, and the pulse waveform. Lin et al. [24] electroplated zinc by using both DC and pulse currents. The utilized pulse frequency was 10, 100, 500 Hz with a duty cycle of 20%. The pulse current was 6 Adm^{-2}. The results show that the finest produced grain was about 33 nm at 10 Hz. The elevation of the frequency to 100 Hz increases the particle size slightly. A further rise of the pulse frequency to 500 Hz reduces the grain size. Besides, the pulse plating provides a finer grain size compared to the conventional DC electroplating.

As mentioned, the reduction of zinc in an electroplating process is a critical step in charging of zinc-air batteries. The optimization of the zinc reduction process directly promotes the energy storage capacity and efficiency of zinc-air batteries. Hence, the present study aims to experimentally optimize the zinc reduction in a pulse electroplating process by optimizing the key influential parameters of the reduction process for the first time. The Taguchi method is utilized to optimize the value of electrolyte temperature, current density, duty cycle, and pulse frequency to maximize the zinc reduction in a charging process. The improvement of zinc reduction by using an optimized chemical process is crucial for practical and commercial application of zinc-air batteries.

2. Experimental

Fig. 2 (a) depicts an actual zinc-air flow battery with separated charging and discharging modules with six charging cells at the top and six discharging cells at the bottom. Each of the reduction cells is made of

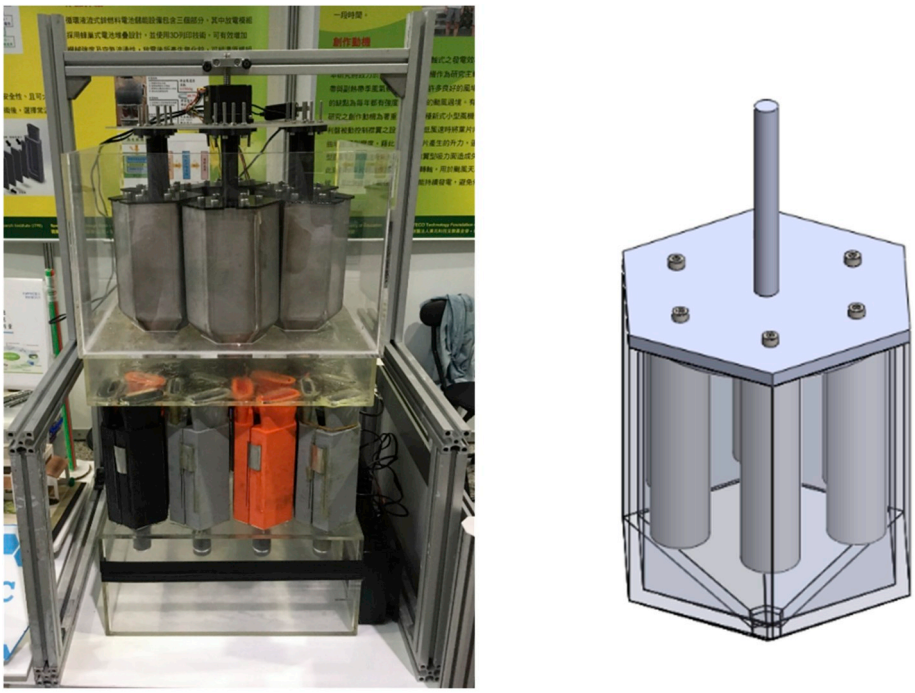

Fig. 2. (a) A practical zinc-air battery with six charging cells at the top and six discharging cells at the bottom; (b) Six poles inside each cell.

a hexagonal funnel-shaped tank containing six immersed reduction anodes (see Fig. 2 (b)) to match six poles in a 100 W charge and discharge energy storage system. As mentioned, the present study aims to optimize the key factors of electrolyte temperature, pulse current, duty cycle, and pulse frequency. Hence, here, to ensure that there are not many unstable factors, the six zinc oxide reduction poles are simplified into only one reduction pole in the current study.

2.1. Experimental setup

A schematic view of the experimental setup is depicted in Fig. 3. As seen, a single pole including an anode and a cathode is placed in an electrolyte container. The poles are connected to a pulse generator power supply. A temperature controller module (SM5-LCD with an accuracy of 0.1 °C) is placed in the electrolyte to control and measure the temperature of the electrolyte during the experiment. The container is placed over a magnetic mixer (P-30; Yeong-Shin Co., Ltd.) to induce a

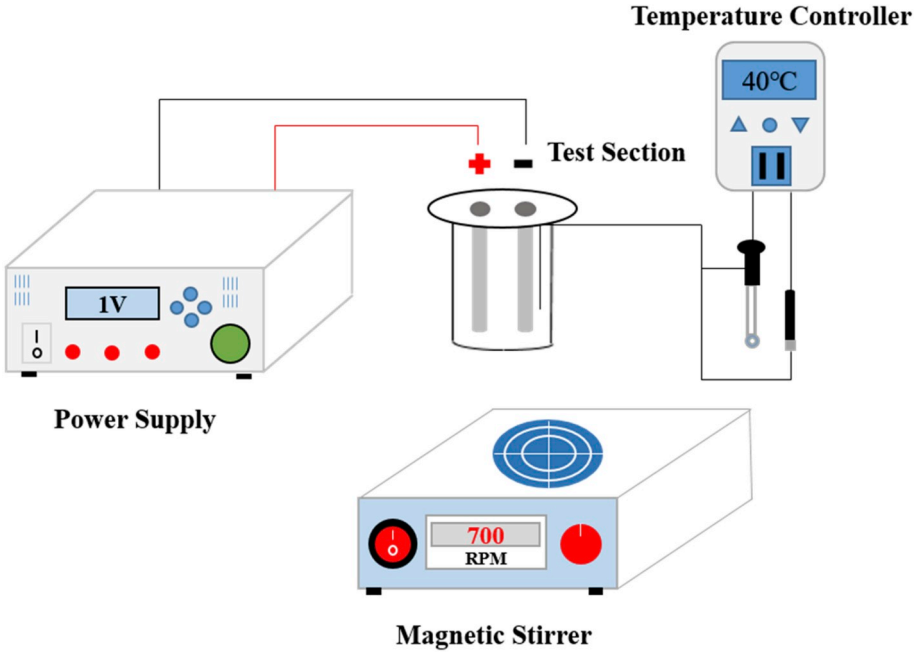

Fig. 3. Schematic view of the experimental setup.

constant flow of electrolyte in the container.

A high electrical conductive road of C1100 toughened copper (with purity 99.9% made of Baoqiao Copper Plate Ltd.) is used as the anode and cathode for the electrodeposition purpose. The diameter and the length of the toughened copper are 19 mm and 100 mm, respectively. In order to connect the experimental module to the circuit, the toughened copper tapped with an M6-sized hole at its tip to a depth of 20 mm.

In order to prevent the corrosion of toughened copper, the copper road was sent to a professional electroplating company to plate a layer of rhodium on its surface uniformly.

A 3,000 ml glass measuring cup is utilized as the electrolyte container. A 3D printer (model Ultimaker 3 Extended; 3DMart Ltd.) is used to print the upper cover of the container to fix the relative distance between the anode and the cathode for the experiment. The distance between the two holes at the cover is 40 mm. After fixing the anode and cathode to the upper cover, the maximum distance between the two poles is 59 mm and the shortest distance is 21 mm.

The electrolyte used for electrodeposition was alkaline electrolyte of 40%wt (10.1 M). Potassium hydroxide particles (with a purity of 95%; First Chemical Co., Ltd.) with a weight of 1,360 g was dissolved in 2,040 g of deionized water to form a potassium hydroxide (KOH) solution. When preparing the potassium hydroxide electrolyte, the quantitative bottle containing the potassium hydroxide electrolyte was placed on a magnet mixer and stirred at 700 rpm until the potassium hydroxide particles are completely dissolved in deionized water. The standard to set the speed of the magnet mixer was that according to the J. C. Chen's paper. As long as there is a certain degree of agitation so that zinc oxide can be uniformly dissolved in the electrolyte, the zinc oxide consumed at the cathode can be quickly replenished.

Since the potassium hydroxide particles release a pungent odor with an exothermic reaction during the dissolution process, the potassium hydroxide electrolyte was synthesized in an extraction cabinet.

2.2. Experimental measurement

There are various control factors in this experiment such as electrolyte temperature, electrodeposition current density, pulse frequency and duty cycle. The duty cycle (D) was introduced as:

$$D = 100 \times T_{on}/(T_{on} + T_{off}) \quad (1)$$

where T_{on} is the duration of the active pulse, and T_{off} is the duration of the inactive pulse.

The pulse frequency (f) is introduced as:

$$f = 1/(T_{on} + T_{off}) \quad (2)$$

The current peak (I_p) can be evaluated as:

$$I_p = I \times (T_{on} + T_{off})/T_{on} \quad (3)$$

where I is the average current.

During each experiment, the voltage value should be monitored. The maximum allowable voltage under different electrodeposition currents should not exceed 2.5 V. If the voltage exceeds 2.5 V, the electrolyte will be electrolyzed, and hydrogen production will be involved in the experiment. Hydrogen production is an undesired phenomenon in the charging process, and it changes the concentration of the electrolyte, causing experimental errors.

The experiment-steps of the present study are summarized in Fig. 4. Following the procedure of Fig. 4, first, a sufficient amount of zinc oxide (Concentration of 99.7%; First Chemical Co., Ltd.) is mixed into the potassium hydroxide electrolyte using a magnetic stirrer to be uniformly mixed for 3 h.

The electrolyte is heated to the desired temperature by setting the temperature module to the experiment temperature. The anode and cathode are immersed in a 40 wt% (10.1 M) KOH electrolyte to commence the experiment. The magnetic-stirrer with a speed of 700 rpm is used to produce a uniform flow of zinc oxide during the experiment. The pulse supply (model ST-2525H; Gitek Electronics Co., Ltd.) was adequately connected to the reduction pole. The experiment was conducted by setting the pulse wave rectification power supply and adjusting the electrodeposition current density, pulse frequency as well as the duty cycle ratio required for the experiment. The electrodeposition time was 1 h. The maximum voltage was recorded during the experiment. After 1 h, the measurement of the reduced Zinc was performed according to the procedure depicted in Fig. 5.

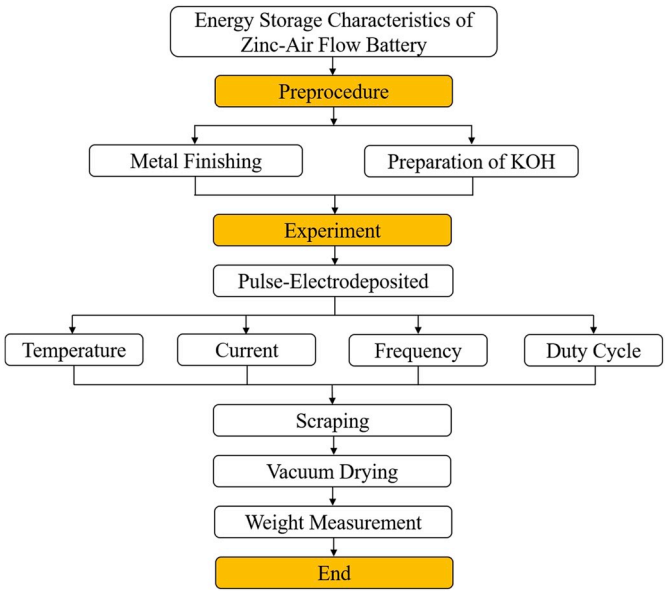

Fig. 4. Experimental procedure for energy storage characteristics of zinc-air flow battery.

The produced zinc particles were scraped from the cathode into a measuring cup. The liquid zinc cup containing the liquid was placed in a vacuum oven (DOV-30 N; Yeong-Shin Co., Ltd.) at 80 °C for 3 h to completely remove the liquid. After baking, the measuring cup was taken out of the oven and was put into a plastic vacuum dish (PC-210; Yeong-Shin Co., Ltd.) and vacuumed by an acid and alkali vacuum pump (90 W; Yeong-Shin Co., Ltd.) to prevent oxidation by contact with air. The weight of the zinc particles was then measured using a high

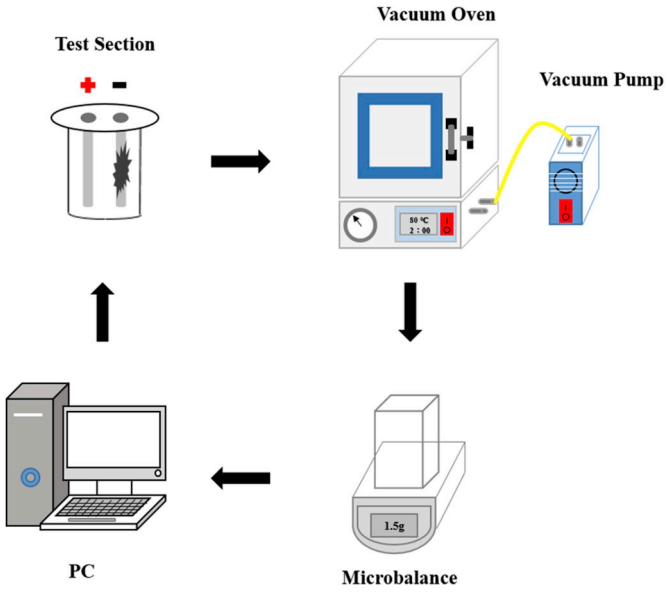

Fig. 5. Experimental procedure for measuring the reduced zinc particles.

precision electronic balance (EHB+150; T-Scale Ltd.). Each experiment was repeated twice, and the average value was reported. The experiment data were transferred into a PC for further process. Each test was conducted for the variables introduced in the experiment table, which will be introduced later.

3. Optimization method

Taguchi method is utilized to analyze the trend of experimental results and optimize the reduction of zinc particles. There are excellence reviews [25,26] on the application of the Taguchi method in the optimization of various process systems and improving products quality. Recently, the Taguchi method has been used for the optimization of nano-composite material [27], mold optimization [28], and laser welding process [29]. The Taguchi method benefits a simple orthogonal table for the set of experiment variables to reduce the number of experimental groups and find out the causes of quality variation. The most important feature of the Taguchi method is that it can configure the level of each design parameter to reduce the number of experiments and find the optimization trend with performing a few tests. The characteristics of the Taguchi method are quality characteristics based on the quality loss function, definition and selection of experimental parameters, signal to noise ratio, and Taguchi orthogonal table. The execution steps of the Taguchi method are illustrated in Fig. 6.

The main steps of the Taguchi method are 1. Establish clear quality characteristics; 2. Determine the target value of the quality characteristics; 3. List all the factors that affect this quality characteristic; 4. Set the level of the signal factor; 5. Set the level of the control factor; 6. If necessary, set the level of the interference factor and perform the interference experiment; 7. Select the appropriate orthogonal table to design a complete experimental plan; 8. Execute the experiment and record the experimental data; 9. Data integration and analysis; 10. Confirm the experiment.

In the present research, the weight of zinc particles is used as the quality characteristic, and Signal to Noise ratio S/N as the quality indicator. Here, the goal is to maximize the zinc production (Maximize the response). Hence, following the Taguchi method, the S/N ratio is introduced as:

$$S \Big/ N = -10\log_{10}\left(\frac{1}{n}\sum_{i=1}^{n}\frac{1}{Yi^2}\right) \quad and\ i = 1\ to\ \ number\ \ of\ \ levels \tag{4}$$

where n denotes the number of observations in the experiment, and Y denotes the respective characteristic.

The control factors that can be expected to actually affect the quality characteristics and can be controlled were selected as electrolyte temperature, electrodeposition current density, pulse frequency, and duty cycle. As the experiments were performed in a controlled environment, it is assumed that there is no interference factor.

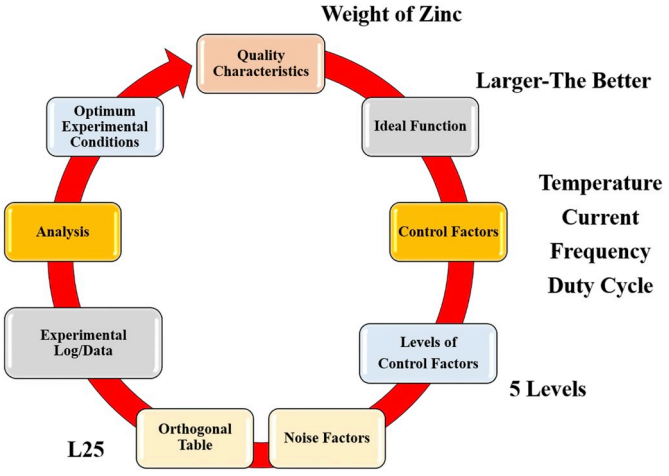

Fig. 6. Steps in the implementation of the Taguchi method.

In the present study, four factors and five levels were used, namely electrolyte temperature, electrodeposition current density, pulse frequency, and duty cycle. The temperature range of the electrolyte is considered to be between 20 °C and 60 °C. The current range is selected initially between 0.7 A and 1.5 A, but it is found that the current of 1.5 A is matched with other parameters. At some levels, the output voltage value exceeds 2.5 V. In order to avoid exceeding the voltage value threshold, the current range is changed to 0.6 A–1.4 A.

A preliminary experiment was conducted for zinc reduction as a function of duty cycle (D) when the temperature, pulse current, and pulse frequency were 40 °C, 1.5 A, and 1,000 Hz, respectively. The results are summarized in Table 1. Table 1 reveals that the duty cycle of 90% has the best benefit under this condition. Any increase or decrease of duty cycle deteriorates zinc reduction. Therefore, the range of 75%–95% was selected as the experimental range of duty cycle for the Taguchi method. In a similar case with temperature 40 °C, current 1.5 A and duty cycle 90%, the variation of the pulse frequency were explored. The corresponding weights of the produced zinc are summarized in Table 2 for pulse frequency in the range of 1 Hz–1,000 Hz. This table shows that the frequency of 100 Hz produces the maximum weight of zinc particles, and any variation of frequency reduces the weight of the produced zinc particles. Therefore, the frequency ranges of 1 Hz–200 Hz is selected for the pulse frequency. The range and level of control parameters are summarized in Table 3.

In the Taguchi method, an orthogonal table shall be introduced to simplify the number of experiments is an experimental plan configuration. In an orthogonal table, the factors and levels are combined in a straight line arrangement. The orthogonality allows the factors to be evaluated individually. The orthogonal table of zinc particle reduction is reported in Table 4, corresponding to four factors and five levels. This table contains 25 experiments and based of the Taguchi method is known as L25. Later, the experiments will be performed for the set of control parameters reported in Table 4. Then, the computed reduction zinc for these set of control parameters will be utilized for calculation of S/N ratio, and finding the optimal parameter combination that will maximize the zinc oxide reduction (energy storage).

4. Results and discussion

Before commencing the experiments for all 25 test sets of Table 4, the feasibility and reproducibility of using this experimental method were tested. The experiment were repeated for three random sets of Table 4, which were raw No. 11th (40 °C, 0.6 A, 100 Hz, 95%), No. 14th (40 °C, 1.2 A, 1 Hz, 85%), and No. 24th (60 °C, 1.2 A, 100 Hz, 80%), and the reduced zinc were measured three times to verify the error value. The experiments were performed using the same control conditions and with the same analysis steps. The results of reproducibility experiments are shown in Table 5. According to the test results, the experimental error of the 11th group is 0.057 g–0.158 g, the experimental error of the 14th group is 0.016 g–0.165 g, and the experimental error of the 24th group is 0.028 g–0.104 g. The measured values of reduced zinc particles in

Table 1
Reduced zinc as a function of the duty cycle for a case of 40 °C, 1.5 A, and 1,000 Hz.

Duty cycle (%)	Zinc weight (g)
95	2.069
90	2.642
85	1.480
80	0.949
75	0.842
70	0.803
60	0.443

Table 2
Reduced zinc as a function of pulse frequency for a case of 40 °C, 1.5 A, and 1 kHz.

Frequency (Hz)	Zinc weight (g)
1	3.568
10	3.968
50	4.120
100	4.788
200	3.891
300	3.795
500	3.550
1000	2.642

Table 3
The range and levels of control parameters.

Factors	Description	Level 1	Level 2	Level 3	Level 4	Level 5
A	Temperature	20 °C	30 °C	40 °C	50 °C	60 °C
B	Current*	0.6 A	0.8 A	1.0 A	1.2 A	1.4 A
C	Frequency	1 Hz	50 Hz	100 Hz	150 Hz	200 Hz
D	Duty Cycle	75%	80%	85%	90%	95%

Current density can be calculated as Current (A)/reaction area (reaction area: 0.4773 dm^2).

Table 4
Taguchi L25 orthogonal table corresponding to range and levels of control parameters.

No.	Factors			
	A	B	C	D
1	20 °C	0.6 A	1 Hz	75%
2	20 °C	0.8 A	50 Hz	80%
3	20 °C	1.0 A	100 Hz	85%
4	20 °C	1.2 A	150 Hz	90%
5	20 °C	1.4 A	200 Hz	95%
6	30 °C	0.6 A	50 Hz	85%
7	30 °C	0.8 A	100 Hz	90%
8	30 °C	1.0 A	150 Hz	95%
9	30 °C	1.2 A	200 Hz	75%
10	30 °C	1.4 A	1 Hz	80%
11	40 °C	0.6 A	100 Hz	95%
12	40 °C	0.8 A	150 Hz	75%
13	40 °C	1.0 A	200 Hz	80%
14	40 °C	1.2 A	1 Hz	85%
15	40 °C	1.4 A	50 Hz	90%
16	50 °C	0.6 A	150 Hz	80%
17	50 °C	0.8 A	200 Hz	85%
18	50 °C	1.0 A	1 Hz	90%
19	50 °C	1.2 A	50 Hz	95%
20	50 °C	1.4 A	100 Hz	75%
21	60 °C	0.6 A	200 Hz	90%
22	60 °C	0.8 A	1 Hz	95%
23	60 °C	1.0 A	50 Hz	75%
24	60 °C	1.2 A	100 Hz	80%
25	60 °C	1.4 A	150 Hz	85%

Table 5
Results of reproducibility experiment.

No.	Times	Zinc weight (g)
11	1	0.253
	2	0.310
	3	0.152
14	1	1.838
	2	1.987
	3	1.822
24	1	0.917
	2	0.841
	3	0.945

Table 5 confirm that the error value generated by this experimental method is relatively small, and the results are reproducible.

Here, the zinc reduction experiments were carried out according to the L25 orthogonal Table 4. Each test was performed twice, and the average value was reported in Table 6. After measuring the produced zinc for all of parameters groups of Table 4, the S/N ratio is calculated following Taguchi method to obtain the individual Level values of the four control factors at the five levels. Later, the results of Table 6 will be utilized to obtain the optimum set of control parameters.

4.1. Influence of control parameters on the S/N factor

The effect of the variation of control parameters on the enhancement of zinc reduction was explored in graphical figures. The influences of temperature, pulse current, pulse frequency, and duty cycle on the N/S ratio are plotted in Fig. 7 (a), (b), (c), and (d), respectively.

Fig. 7(a) shows that the increase of temperature from 20 °C to 40 °C improves S/N ratio from −5.76 dB to an optimum value of 1.257 dB, and a further increase of temperature reduces the S/N ratio. The S/N ratio drops to −10.145 dB by the rise of temperature to 60 °C. During the reduction experiment, it is found that as long as the temperature of the electrolyte is raised to above 50 °C, the zinc particles produced by any control factor are relatively tight and difficult to scrape. The reason is that the increase of the temperature accelerates the electrodeposition reaction at the cathode. The diffusion rate of ions reduces the polarization at the cathode, and hence, the plating layer is fine and tight [16, 17]. The trend of the results in Fig. 7(a) shows that the control of the electrolyte temperature is an essential factor, affecting the energy storage characteristics of zinc oxide reduction. The use of an appropriate electrolyte temperature helps to improve the zinc oxide reduction efficiency and obtain a softer zinc particle. A further increase in the temperature reduces the energy storage and makes the scraping of zinc particles hard. The ease of scraping of zinc particles is an advantage because the generated zinc particles need to be scraped off and sent back to the discharge end of the system in the actual flow battery. Therefore, an optimum temperature of 40 °C is adequate for systems of zinc air flwo batteries with the benefit of energy storage efficiency and ease of

Table 6
Average value of two experimental results of the Taguchi method (L25).

No.	Factors					
	Temperature (°C)	Current (A)	Frequency (Hz)	Duty Cycle (%)	Zinc weight (g)	*S/N* (dB)
1	20	0.6	1	75	0.138	−17.255
2	20	0.8	50	80	0.269	−11.411
3	20	1.0	100	85	0.478	−6.422
4	20	1.2	150	90	1.338	2.529
5	20	1.4	200	95	1.548	3.781
6	30	0.6	50	85	0.750	−2.500
7	30	0.8	100	90	0.691	−3.217
8	30	1.0	150	95	0.708	−3.000
9	30	1.2	200	75	0.902	−0.895
10	30	1.4	1	80	1.359	2.664
11	40	0.6	100	95	0.282	−11.144
12	40	0.8	150	75	0.787	−2.125
13	40	1.0	200	80	1.569	3.912
14	40	1.2	1	85	1.913	5.612
15	40	1.4	50	90	3.174	10.028
16	50	0.6	150	80	0.020	−34.414
17	50	0.8	200	85	0.281	−11.046
18	50	1.0	1	90	0.783	−2.156
19	50	1.2	50	95	1.533	3.698
20	50	1.4	100	75	1.217	1.688
21	60	0.6	200	90	0.060	−26.596
22	60	0.8	1	95	0.122	−18.739
23	60	1.0	50	75	0.423	−7.566
24	60	1.2	100	80	0.879	−1.145
25	60	1.4	150	85	1.467	3.318

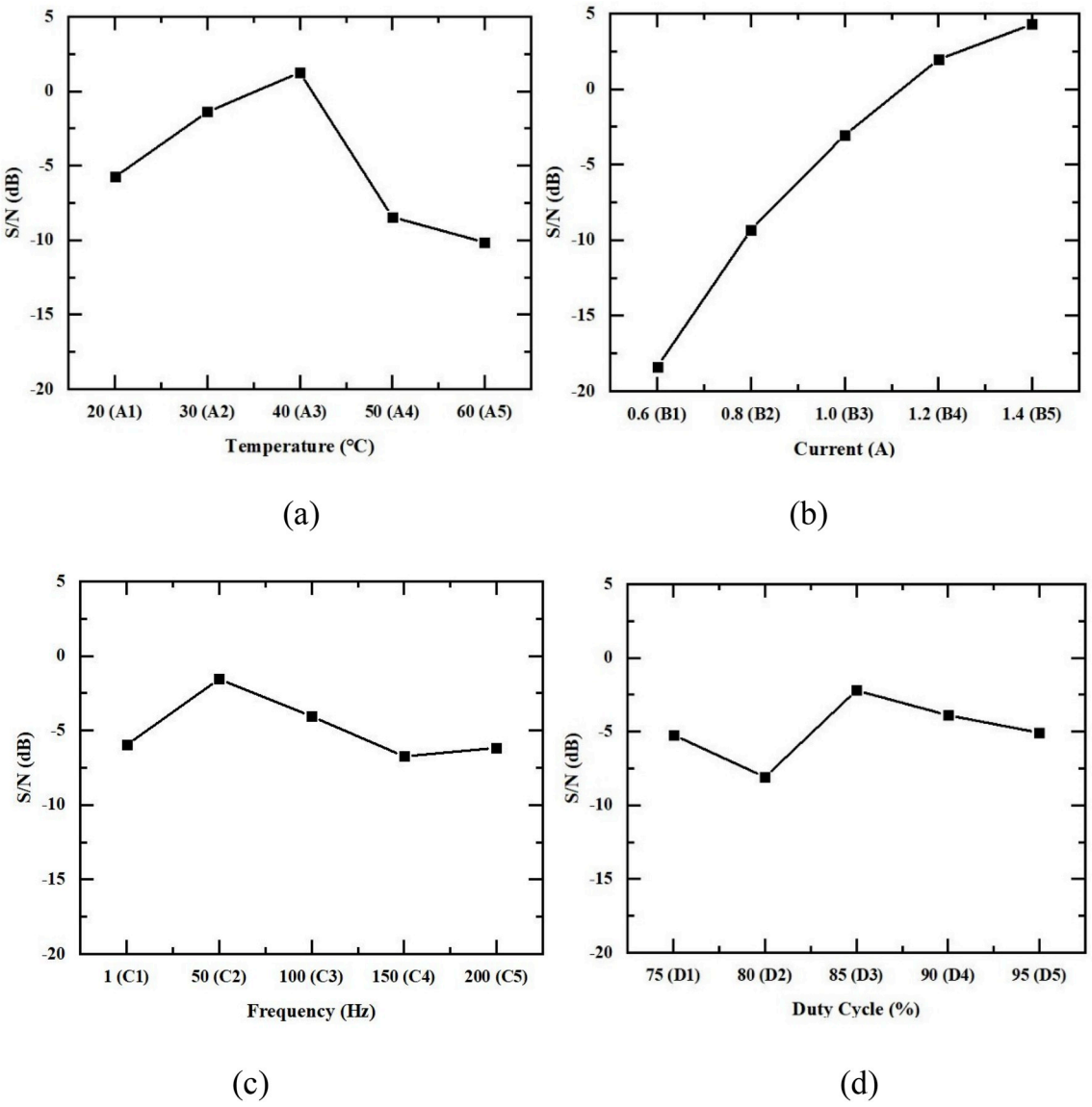

Fig. 7. Influence of control parameters on S/N ratio for reduction of zink. (a) Temperature; (b) Pulse current; (c) Pulse frequency; (d) Duty cycles.

particle recovery.

Fig. 7(b) displays the effect of pulse current on energy storage of zinc oxide reduction. This figure shows that the increase of pulse current increases the zinc reduction (S/N ratio). Since the threshold voltage of KOH electrolyte is 2.5 V, the current value of the supply should be carefully selected. Using a pulse current about 1.5 A results in an output voltage higher than the critical voltage value of 2.5 V. The examined pulse currents were taken from five levels of 0.6 A, 0.8 A, 1.0 A, 1.2 A, 1.4 A.

It should be noted that these currents are the power supply currents. The cathode diameter is 0.19 dm, and the cathode column height in contact with the KOH electrolyte is 0.8 dm. The reaction area between the cathode and the liquid is: 0.4773 dm^2; hence, the pulse current can be converted to current density by dividing the pulse current by surface area, which results in the following current densities 1.257 Adm^{-2}, 1.676 Adm^{-2}, 2.096 Adm^{-2}, 2.515 Adm^{-2}, 2.934 Adm^{-2} corresponding to five current levels of this study. The response graph plotted in Fig. 7 (a) illustrates that the pulse current has a considerable influence on the zinc oxide reduction efficiency. When the current density is continuously increased from 0.6 A to 1.4 A, the S/N ratio is increased from −18.382 to 4.296, and the energy storage efficiency is improved. Therefore, the increase of current density helps to improve the amount of zinc oxide reduction. The reason is that when the current density increases, the potential is higher, the diffusion rate of ions will be significantly increased, and the rate of crystallization can be promoted [19]. However, special attention should be paid to the fact that different electrolytes have limitations on current density. If the current density exceeds the critical value of the current density, the output voltage can be higher than the critical voltage value, which may lead to hydrogen evolution of the electrolyte and hydrogen bubble generation [30].

Fig. 7(c) depicts the effect of pulse frequency on the S/N ratio of zinc oxide reduction for five frequency levels of the Taguchi method. According to the factor response graph plotted in Fig. 7(c), the pulse frequency has a relatively gentle effect on the reduction efficiency relative to the electrolyte temperature and the current density. When the frequency is gradually increased from 1 Hz to 50 Hz, the S/N ratio increases from −5.975 dB to −1.550 dB, which is the best energy storage characteristics. However, as the pulse frequency continues to increase from 50 Hz to 200 Hz, the S/N ratio is reduced to a level close to 1 Hz. The reason is that when the pulse frequency is low, a large peak-current can be generated, that sharply reduces the ion concentration near the cathode during one pulse time, and hence, the metal deposition can occur faster. Therefore, the pulse frequency can be appropriately adjusted according to different electrolyte solutions to improve the

current-peak, and the quality of the plating layer. The electrodeposition efficiency can be changed according to application needs by adjusting the pulse frequency [31].

Fig. 7(d) shows the effect of duty cycle on the S/N ratio of zinc oxide reduction for energy storage enhancement. A total of five levels, 75%, 80%, 85%, 90%, 95%, were used to determine the degree of influence of the pulse cycle using the Taguchi method. From the factor response graph (Fig. 7(d)), it can be seen that when the duty cycle is increased from 75% to 85%, the S/N ratio is first decreased from −5.231 dB to −8.779 dB, and then raised to −2.007, which gives the best reduction benefit. When the pulse cycle rises to 95%, the S/N ratio drops to −5.81, which means that the energy storage efficiency drops to a level close to the duty cycle of 75%. This is because the duration values of the active pulse and inactive pulse affect the formation rate and growth rate of the coating crystal. The high deposition rate during an active pulse causes the ion concentration near the cathode to drop rapidly. The relatively long inactive pulse duration allows the ions to have sufficient time to replenish the ions consumed at the cathode and restore their concentration to provide the next pulse plating [3]. In the present experiment, a magnetic mixer accelerates the dissolution of zinc oxide and solution diffusion, and hence, the ion concentration can be balanced without the requirement of a long inactive pulse.

4.2. Taguchi analysis and optimization solution

After performing all of the experiments introduced in L25 table, a subsequent analysis can be carried out by combining the S/N ratios of the electrolyte temperature, current density, pulse frequency, and duty cycle to find the Taguchi optimized set of control parameters. The four factors, affecting the proportion of the results, are listed in the factor response table, as shown in Table 7. In this table, the Level value is the average of the S/N ratio of the control factor at the level. For example, the Level 1 value of the A factor is the average of S/N ratio for A factor at the first level, and so on. The Delta value is the difference between the maximum value and the minimum value among the five Level values of each control factor. For example, the value of Delta in column A is (1.257 dB) - (−10.145 dB) = 11.402 dB, and the rest of the Delta values are calculated in the same way.

The Rank value sorts the Delta values in order according to the size of Delta values. As shown in Table 7, the Rank of the control factor B is 1, which means that the control factor B is ranked first when the amount of zinc particles is used as the quality characteristic. Following the ranks of Table 7, Taguchi method shows that (1) Current density, (2) electrolyte temperature, (3) duty cycle, and (4) Pulse frequency are the control parameters, affecting the enhancement of zinc reduction, by order of significance.

Now, the optimal level of the four factors can be obtained from the individual factor response graphs, as shown in Fig. 7. Using Fig. 7, the optimum values of control parameters are electrolyte temperature at the third level −40 °C, the current density at the fifth level −1.4 A (2.934 Adm^{-2}), the pulse frequency at the second level −50 Hz, and the duty cycle at the third level of −85%. The zinc reduction was measured twice for the optimized combination of parameters in the same experimental procedure. The weight of the produced zinc particles was as 3.607 g and 3.728 g. Therefore, the average weight of zinc reduction is 3.668 g.

The best parameter combination in the T25 experiment of Taguchi method was the row No. 15th with the average 3.174 g produced zinc particles. The worst combination of the L25 experiment is the row No. 16th with 0.02 g produced zinc particles.

In order to prove that under the same experimental conditions, the use of pulse plating method can help to improve the reduction efficiency of zinc oxide compared with DC electroplating a further test was performed with a DC current. The same electrolyte temperature and current are selected as the combination of pulse plating optimization parameters, and the experiment was repeated twice. The experimental results showed that the weight of the produces zinc particles was 2.338 g and 2.210 g. Hence, the average weight of produced zinc by using DC electroporation was calculated as 2.274 g. The weight of the produced zinc particles for the best (No. 15th) and worst (No. 16th) cases of L25 table, the optimum control parameters proposed by Taguchi method, and the DC method are summarized in Table 8 for comparison purpose. The difference between the weight of the produced zinc by the best set of L25 Table 15th and the optimum set of control parameters is 0.498 g.

The pulse frequency and the duty cycle are two parameters which can control the peak current and crystal growth rate. An increase in the peak current increases the crystal formation, and the crystal formation will be faster than the crystal growth rate. Hence, finer metal particles are generated by using the pulse current [32]. Therefore, the frequency and duty cycle can be appropriately adjusted according to different plating metal solutions, and the rate of crystal formation, and hence, the rate of particle production can be increased. The frequency can be adjusted to improve the efficiency and quality of the coating. The peak current can be changed without exceeding the critical value of the electrolyte voltage and current. Compared with DC electroplating method, the optimized combination of the pulse electroplating provides an additional zinc production of 1.394 g, which proves that the regulation of pulse current frequency and duty cycle does help to enhance the energy storage and reduction of zinc oxide at the same electrolyte temperature and current density.

4.3. Electrodeposition surface analysis

In addition to the examination of the weight of the produced zinc particles by direct current and pulse plating, the surface texture and produced particles are also investigated. A scanning electron microscopy is utilized to analyze the electrodeposition surface. The surface analysis was performed for the optimized set of control parameters (a), DC plating (b), and the worst case of L25 table (No. 16th). The results are illustrated in Fig. 8. The SEM photos are depicted for two shooting magnification of 1,000 times and 3,000 times.

At 1,000 times magnification, Fig. 8(a) clearly shows that many loose fine zinc particles are crystallized together and formed some branches. There are many void spaces between the branches. The appearance of zinc particles of Fig. 8(b) is obviously different from that in Fig. 8 (a). The crystals are combined like clay into a rock-like pattern, showing a rugged and thick appearance, rather than a small appearance. Fig. 8(c) shows that the crystalline form is similar to that of Fig. 8(a). The elongated dendritic zinc particle crystals are grouped together to form a reef-like shape with several pores between the crystals.

Table 7
The calculated factor responses, S/N (dB).

No.	A	B	C	D
	Temperature	Current	Frequency	Duty
Level 1	−5.756	−18.382	−5.975	−5.231
Level 2	−1.390	−9.308	−1.550	−8.079
Level 3	1.257	−3.046	−4.048	−2.207
Level 4	−8.446	1.959	−6.738	−3.882
Level 5	−10.145	4.296	−6.169	−5.081
Delta	11.402	22.677	5.188	5.871
Rank	2	1	4	3

Table 8
Comparison between DC plating and pulse plating.

No.	Factors				
	Temperature	Current	Frequency	Duty	Zinc weight
15	40 °C	1.4 A	50 Hz	90%	3.174 g
Optimum	40 °C	1.4 A	50 Hz	85%	3.668 g
Worst	50 °C	0.6 A	150 Hz	80%	0.02 g
DC	40 °C	1.4 A	–	–	2.274 g

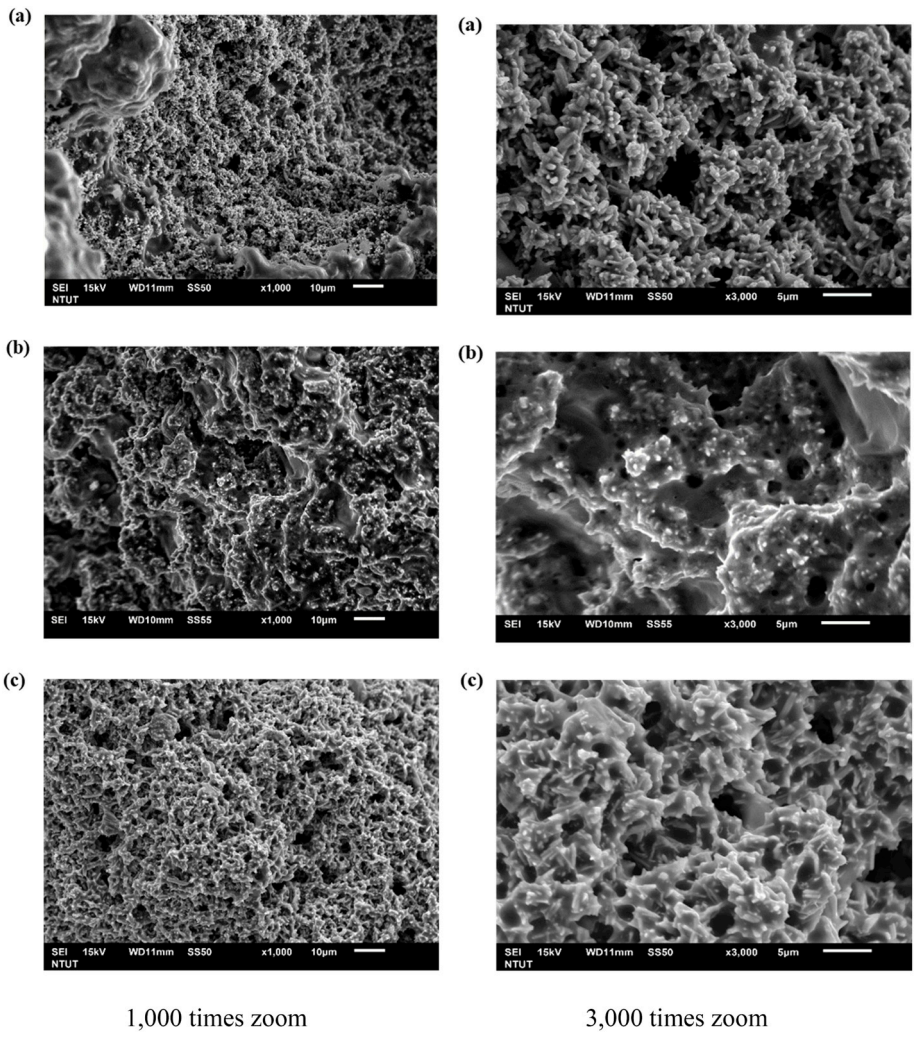

Fig. 8. The surface SEM photo (a) Optimized combination; (b) DC plating; (c) L25 orthogonal table worst combination (No. 16th) for two shooting zooms of 1,000 times and 3,000 times.

At 3,000 times magnification, the crystal morphology of the fine particles, which were observed in Fig. 8(a) with 1,000 times magnification, can be more clearly seen for the optimized configuration in Fig. 8 (a) with 3,000 times magnification. Many elongated particles grow out around the larger crystals, like cactus, and there are obvious gaps between the crystals. Fig. 8(b) shows that the crystals are in a massive form with a few pores on the surface and the sharp-formed zinc particles crystallizing. A new formation can also be seen from the surface of Fig. 8 (c). In Fig. 8(c), the fine crystals, the number of newly formed crystals is between the optimized combination and the DC plating, and the degree of agglomeration is also between the two.

The peak current of the optimized combination and the worst combination experiment is calculated by Eq. (1). In the case of the optimized combination, the average current was 1.4 A, pulse frequency 50 Hz, duty cycle 85%. Considering, a pulse waveform, the active time of a pulse is 17 ms, and the peak current is 1.647 A. In the case of the worst combination (No. 16th), the average current is 0.6 A, the pulse frequency is 150 Hz, and the duty cycle is 80%. The active time of a pulse is 5.33 ms, and the peak current is 0.75 A. The peak current value of DC plating is 1.4 A equal to the average current. By using a pulse current, the peak current value can be increased to a value higher than the average current value. Rise of the peak current accelerates the crystal formation, and the crystal formation can occur faster than crystal growth. Thereby, the pulse current affects the crystallization type by producing finer crystals.

5. Conclusion

The zinc reduction is an essential part of a zinc-air flow battery which occurs in the charging module of the battery. During the charging process, the zinc-oxide reduces to zinc particles at the cathode surface, and the recovered zinc can be later consumed in the discharge module of the battery. Therefore, the reduction of zinc in a zinc-air flow battery is equivalent to the electrical energy storage in the battery. Any increase in zinc reduction directly increases the energy storage in the battery during the charging process. In the present study, a rectified pulse current with an adjustable pulse current, a pulse frequency, and a duty cycle is utilized to recover zinc from zinc oxide dissolved in KOH electrolyte experimentally. Taguchi method is employed to maximize the zinc reduction during the charging process. The electrolyte temperature, pulse current, pulse frequency, and duty cycle were adopted as the controlling parameters of the Taguchi method. Following the Taguchi method, the zinc reduction was selected as the quality characteristics to be maximized. For four control parameters, five levels were adopted. The experiments were performed for an orthogonal table of parameters and levels with the size of L25. The main outcomes of the study can be summarized as follows:

1 There is an optimum temperature of 40 °C for zinc reduction. This temperature not only optimizes the zinc reduction but also produces fine zinc particles. Producing fine zinc particles is an advantage in

changing process of a zinc-air flow battery as it facilities the mechanical process of zinc recovery.

2 The optimum values of the pulse frequency and duty cycle were found as 50 Hz and 85%, respectively. Using a well-adjusted pulse frequency and duty cycle provides an opportunity of peak current and zinc ion balance at the cathode, which enhanced the zinc recovery.

3 Using an optimized value of control parameters (temperature 40 °C, current 1.4 A, frequency 50 Hz, duty 85%) produces 3.668g zinc during 1 h of charging.

4 The experiment was repeated with the electrolyte temperature (40 °C) and current (1.4 A) the same as the optimum case but with a DC current instead of the pulse current. The reduced zinc for the DC current was 2.274g. Comparison of this amount of recovered zinc with the optimum value of 3.668g shows that using a pulse current significantly enhances the zinc recovery and energy storage efficiency of zinc-air flow batteries.

5 The SEM images of the produced zinc particles show that using the optimum current pulse indicates that the many zinc particles are crystallized together and formed some branch shapes. Around each large crystal, some tiny zinc particles are forming a cactus shape.

In the present study, a pulse current in the form of a square wave was used to charge the zinc-air battery module, and the results demonstrate the advantage of using a pulse current over a usual DC current. Study of other wave shapes such as sine waves, saw-tooth waves, and triangular waves for pulse current can be subject of future works.

Acknowledgments

The authors appreciate the financial support from Ministry of Science and Technology, Taiwan, under grant number MOST 106-2221-E-027-103. The authors also appreciate the financially supported by the “Research Center of Energy Conservation for New Generation of Residential, Commercial, and Industrial Sectors” from The Featured Areas Research Center Program within the framework of the Higher Education Sprout Project by the Ministry of Education (MOE) in Taiwan.

References

[1] H. Zheng, C. Wang, Q. Liu, Z. Tian, X. Fan, Energy Convers. Manag. 157 (2018) 372–381.
[2] A.R. Mainar, O. Leonet, M. Bengoechea, I. Boyano, I. de Meatza, A. Kvasha, A. Guerfi, J. Alberto Blázquez, Int. J. Energy Res. 40 (2016) 1032–1049.
[3] Z. Xue, W. Lei, Y. Wang, H. Qian, Q. Li, Surf. Coat. Technol. 325 (2017) 417–428.
[4] S. Clark, A. Latz, B. Horstmann, Batteries 4 (2018) 5.
[5] M.A. Rahman, X. Wang, C. Wen, J. Electrochem. Soc. 160 (2013) A1759–A1771.
[6] J. Wang, Y. Li, X. Sun, Nano Energy 2 (2013) 443–467.
[7] M. Kar, B. Winther-Jensen, M. Forsyth, D.R. MacFarlane, Phys. Chem. Chem. Phys. 15 (2013) 7191–7197.
[8] J. Fu, Z.P. Cano, M.G. Park, A. Yu, M. Fowler, Z. Chen, Adv. Mater. 29 (2017) 1604685.
[9] W. Hong, H. Li, B. Wang, Int. J.Electrochem. Sci. 11 (2016) 3843–3851.
[10] P.-C. Li, Y.-J. Chien, C.-C. Hu, J. Power Sources 313 (2016) 37–45.
[11] C.A. Friesen, R. Krishnan, G. Friesen, in, Google Patents, 2013.
[12] S. Amendola, L. Johnson, M. Binder, M. Kunz, P.J. Black, M. Oster, S. Sharp-Goldman, T. Chciuk, R. Johnson, in, Google Patents, 2013.
[13] J. Fu, J. Zhang, X. Song, H. Zarrin, X. Tian, J. Qiao, L. Rasen, K. Li, Z. Chen, Energy Environ. Sci. 9 (2016) 663–670.
[14] J. Fu, D.U. Lee, F.M. Hassan, L. Yang, Z. Bai, M.G. Park, Z. Chen, Adv. Mater. 27 (2015) 5617–5622.
[15] U. Sahaym, S.L. Miller, M.G. Norton, Mater. Lett. 64 (2010) 1547–1550.
[16] L. Jinlong, L. Tongxiang, W. Chen, J. Solid State Chem. 240 (2016) 109–114.
[17] M. Yamaguchi, H. Yamamuro, M. Takashiri, Curr. Appl. Phys. 342 (2018) 121–128.
[18] M. Kazazi, Ceram. Int. 44 (2018) 10863–10870.
[19] D.V. Kumar, M. Prasad, Surf. Coat. Technol. 342 (2018) 121–128.
[20] F. Walsh, C. Low, Surf. Coat. Technol. 304 (2016) 246–262.
[21] A. Lelevic, F.C. Walsh, Surf. Coat. Technol. 369 (15 July 2019) 198–220.
[22] H. Yang, E.O. Fey, B.D. Trimm, N. Dimitrov, M.S. Whittingham, J. Power Sources 272 (2014) 900–908.
[23] R. Chandran, S.K. Panda, A. Mallik, Mater.Renew.Sustain. Energy. 7 (2018) 6.
[24] H. Lin, C. Ho, C. Lee, Surf. Coat. Technol. 319 (2017) 378–385.
[25] N.C. Fei, N.M. Mehat, S. Kamaruddin, ISRN.Ind. Eng. (2013) 2013.
[26] R. Jeyapaul, P. Shahabudeen, K. Krishnaiah, Int. J. Adv. Manuf. Technol. 26 (2005) 1331–1337.
[27] P. Madhukar, N. Selvaraj, C. Rao, V.K. GB, Compos. B Eng. (2019) 107136.
[28] K.M. Hyie, S. Budin, M. Wahab, in: IOP Conference Series: Materials Science and Engineering, IOP Publishing, 2019, 012060.
[29] K. Oussaid, A. El Ouafi, A. Chebak, J. Mater. Sci. Chem. Eng. 7 (2019) 16–31.
[30] A. Sharma, S. Bhattacharya, R. Sen, B. Reddy, H.-J. Fecht, K. Das, S. Das, Mater. Char. 68 (2012) 22–32.
[31] C.-K. Chung, W. Chang, Microsyst. Technol. 13 (2007) 537–541.
[32] M. Uysal, T. Cetinkaya, A. Alp, H. Akbulut, Appl. Surf. Sci. 334 (2015) 80–86.